



Fuel cell system with sodium borohydride as hydrogen source for unmanned aerial vehicles

Kyunghwan Kim^a, Taegy Kim^b, Kiseong Lee^c, Sejin Kwon^{a,*}

^a Department of Aerospace Engineering, School of Mechanical, Aerospace and Systems Engineering, KAIST, 335 Gwahangno, Yuseong-gu, Daejeon 305-701, Republic of Korea

^b Department of Aerospace Engineering, Chosun University, 335 Gwahangno, Yuseong-gu, Daejeon 305-701, Republic of Korea

^c NES & TEC Co., Ltd, 335 Gwahangno, Yuseong-gu, Daejeon 305-701, Republic of Korea

ARTICLE INFO

Article history:

Received 5 November 2010

Received in revised form

24 December 2010

Accepted 12 January 2011

Available online 21 January 2011

Keywords:

Unmanned aerial vehicle (UAV)

Fuel cell

Sodium borohydride

Power management

ABSTRACT

In this study, we design and fabricate a fuel cell system for application as a power source in unmanned aerial vehicles (UAVs). The fuel cell system consists of a fuel cell stack, hydrogen generator, and hybrid power management system. PEMFC stack with an output power of 100 W is prepared and tested to decide the efficient operating conditions; the stack must be operated in the dead-end mode with purge in order to ensure prolonged stack performance. A hydrogen generator is fabricated to supply gaseous hydrogen to the stack. Sodium borohydride (NaBH_4) is used as the hydrogen source in the present study. $\text{Co}/\text{Al}_2\text{O}_3$ catalyst is prepared for the hydrolysis of the alkaline NaBH_4 solution at room temperature. The fabricated Co catalyst is comparable to the Ru catalyst. The UAV consumes more power in the takeoff mode than in the cruising mode. A hybrid power management system using an auxiliary battery is developed and evaluated for efficient energy management. Hybrid power from both the fuel cell and battery powers takeoff and turning flight operations, while the fuel cell supplies steady power during the cruising flight. The capabilities of the fuel-cell UAVs for long endurance flights are validated by successful flight tests.

© 2011 Elsevier B.V. All rights reserved.

1. Introduction

Future combat system and brigade combat team (FCS/BCT) are combat strategy programs that are employed to minimize human losses while maximizing combat efficiency. They consist of manned and unmanned systems controlled by battlefield networks. Small unmanned aerial vehicles (UAVs), which are key components of FCS, have been the main focus of researches in defense and security fields.

UAVs have long been used for surveillance and reconnaissance missions. Flight endurance is the most important factor for improving the mission performance, and hence, the power source of UAVs should have high energy density and high efficiency in order to increase the flight endurance. Low acoustic and heat emissions are also required to avoid detection by enemies. Many researches have been conducted on UAVs [1]. However, their power systems are completely dependent on internal combustion engines or secondary batteries. Internal combustion engines have low thermal efficiency and noise, and high heat emission. These characteristics are not appropriate for military applications. Furthermore, secondary batteries lead to limitations in the mission range due to low energy density. Recently, fuel cell systems have been studied

as alternative power sources for UAVs operating between developed countries [2]. The fuel cell has a simple configuration and high energy density and high efficiency because chemical energy is converted directly to electric energy. In addition, they have no noise and vibration systems.

Gaseous hydrogen is required to operate proton exchange membrane fuel cells (PEMFCs). Hydrogen storage systems comprise a large proportion of the weight of fuel cell systems, and hence, it is important to choose an appropriate hydrogen source. In case of compressed hydrogen and metal hydrides, they are too bulky and heavy to satisfy the required energy density. Chemical hydrides have distinguished as new hydrogen sources due to the high energy density. Especially NaBH_4 alkaline solution has additional advantages: stable, nonflammable, non-toxic, and high hydrogen capacity (10.8 wt.%). In addition, it is easy to control the hydrogen generation by catalytic hydrolysis in terms of system management.

In this study, we have aimed to develop a power source to improve the flight endurance of UAVs. The design and fabrication of a fuel cell system as a power source for UAVs have been conducted. The fuel cell system consisted of three subsystems—a fuel cell stack, hydrogen generator, and hybrid power management system. A PEMFC was selected since it has high efficiency, fast responses to loads, and stable output power for vehicular and mobile applications. A high hydrogen weight density is required to meet the overall energy density of UAVs. Sodium borohydride (NaBH_4) was selected as the hydrogen source. The hydrogen was

* Corresponding author. Tel.: +82 42 350 3721; fax: +82 42 350 3710.
E-mail address: trumpet@kaist.ac.kr (S. Kwon).

generated by a catalytic hydrolysis reaction. A lithium battery was used as a hybrid system for effective power management. The fuel cell system was integrated with the UAV test platform and flight tests were conducted.

2. System description and experimental setup

2.1. Unmanned aerial vehicle (UAV) test platform

We have designed a UAV platform to determine and evaluate the performance of the fuel cell system. The platform was a glider type that is favorable for long-endurance flights. Small UAVs are often launched by hand to gain an impellent power because of the lack of launching and landing spaces in battlefields. Therefore, our glider was designed to be launched by hand and to land by a stall effect; in this technique, the lift force reduces as the angle of attack increases. The specifications are listed in detail in Table 1. Its gross takeoff weight including the fuel payload was 2.5 kg, and it consumed powers of 80 W and 300 W for cruising and takeoff, respectively. The normal power output of the fuel cell system was designed as 80 W for cruising, and its total system weight was limited to a payload of 1.5 kg.

2.2. Fuel cell system design

The fuel cell system was a power source system equipped in the UAV platform. It consisted of the following three major parts—the stack, hydrogen generator, and hybrid power management system; see Fig. 1. The normal output of the fuel cell stack was 80 W, and this corresponds to the power consumption for cruising. The hydrogen generator comprised five main parts: (a) fuel cartridge; (b) micropump; (c) catalytic reactor; (d) gas–liquid separator; and (f) dehumidifier. As mentioned previously, a Li battery was selected for the hybrid power management. The operating principle is as follows: alkaline NaBH_4 solution was fed to the catalytic reactor by using a micropump, and the fuel decomposed into gaseous hydrogen and liquid borate (NaBO_2) by catalytic hydrolysis. The by-product borate was separated in a gas–liquid separator. The generated hydrogen was purified by a dehumidifier and supplied to the stack. Finally, the propulsion module was powered by the stack and Li battery.

Table 1
Specifications of glider platform for fuel cell tests.

Property	Value
Wingspan (m)	2
Length (m)	1.08
Aspect ratio	10
Empty weight of plane (kg)	0.858
Payload (kg)	1.5
Cruising speed (km h^{-1})	40–50

2.2.1. Stack operating modes

The operating modes of a fuel cell can be classified into the flow-through mode and the dead-end mode [3]. The coefficients of utilization of hydrogen for the dead-end and flow-through modes are almost 1 and >1 , respectively, and in the latter, the remaining hydrogen is vented. The dead-end mode is an attractive option for operating the portable fuel cells because of the high fuel utilization [4,5]. However, additional equipments are required to prevent the flooding in the UAV, which is an issue because weight is a key constraint in UAVs. Hence, stack performance tests were conducted with both operating modes to understand the gains and losses in accordance.

The H-100 commercial product (Horizon Fuel Cell Technologies) was prepared in the form of a 100-W PEMFC stack; it comprised 24 single cells, each single cell had 19.2 cm^2 active area, and the cathode channel was the air-breathing type. The normal output power was 100 W at 12.5 V and 8 A, while the open circuit voltage was 20.5 V. In order to find an operating mode that remains stable over a long period of time, performance evaluations were conducted at a constant power mode of 100 W operated by an electric load (3311D, VizzKorea Inc.). Hydrogen was fed from a compressed hydrogen tank, and its purity was 99.999%. A mass flowmeter (FVL-1600A, Omega) was used to measure the flow rate of hydrogen. A solenoid valve, which was 30 g and consumed 2 W, was prepared and the anode channel was purged once every 10 s in the dead-end mode.

2.2.2. NaBH_4 catalytic hydrolysis

Pure hydrogen with no carbon impurities can be obtained by hydrolysis [6,7]. The hydrolysis reaction of NaBH_4 is



Hydrogen is the only gas product in the reaction, and pure hydrogen is obtained after separating the borate byproduct. Kreevoy and Jacobson have reported that the hydrolysis of NaBH_4 depends on pH and temperature in the following manner [7]:

$$\text{Log}_{10} t_{1/2} = \text{pH} - (0.034T - 1.92) \quad (2)$$

Here $t_{1/2}$ is the half-life for the self-hydrolysis of the NaBH_4 solution (min); pH, the hydrogen chemical activity; and T , the storage temperature (K). Hence, it is more effective for the aqueous NaBH_4 solution to exist in an alkaline state with $\text{pH} > 12$ in order to prevent its self-hydrolysis. 15 wt.% NaBH_4 alkaline solution was prepared and it comprised 15 wt.% NaBH_4 , 5 wt.% NaOH , and 80 wt.% water. Sodium hydroxide (NaOH) was used to restrain the self-hydrolysis of NaBH_4 solution.

According to a previous study, noble metals such as Pt, Ru, and Pd have been selected due to their high activity with respect to NaBH_4 hydrolysis reaction [8]. However, these are costly materials. Jeong et al. have reported that Co has high activity with NaBH_4 hydrolysis [9]. Hence, Co has been selected as the catalyst material in the present study. As the catalyst support, gamma-type alumina

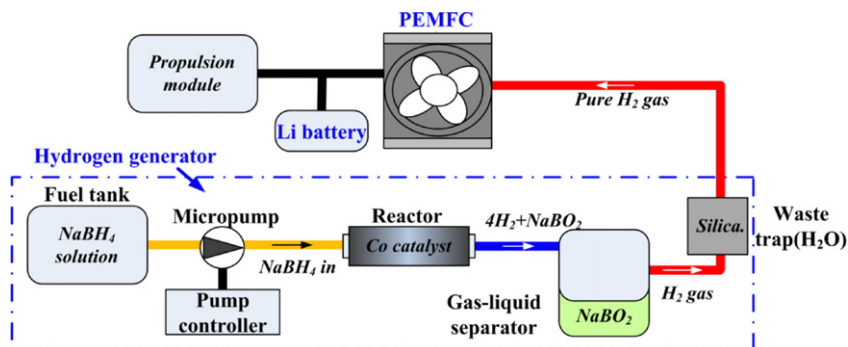


Fig. 1. Operating principle of fuel cell system.

(Al₂O₃) was selected since it has a large surface area per mass ratio. The catalyst was loaded on the Al₂O₃ pellets by a wet impregnation method. The catalyst fabrication procedures can be classified into 4 steps: (a) washing; (b) loading; (c) calcination; and (d) reduction. The alumina was washed in distilled water, and dried at 150 °C for 12 h in order to remove the water and hydroxyl groups. Further, it was immersed in a CoCl₂ precursor solution at room temperature for 24 h and dried again. Calcination procedures were performed at 350 °C for 3 h in order to eliminate the impurities. Reduction was followed to activate Co.

The catalysis was completed after a reduction procedure that activated the activation point of Co.

We fabricated a hydrogen generator comprising a fuel cartridge, micropump, reactor, gas–liquid separator, and dehumidifier. A micro annular geared pump (2521, Micropump, Inc.), which was only 56 g and consumed 3 W, was employed to supply NaBH₄ solution to a Co/Al₂O₃ reactor. The feeding rate was 3 ml min⁻¹ corresponding to 1071 ml min⁻¹ gaseous hydrogen, which represents the hydrogen consumption rate to generate 85 W at the stack.

2.2.3. Power management

Fuel cells have high energy density but low power density. Hence, they should be larger and heavier for applications such as UAVs and vehicles that are operated within a wide power range. Hence, it is more effective to use a hybrid system in high-power consumption regions. A hybrid power management system, which has compatible modules with an auxiliary battery, has been employed to meet high power consumption operational requirements such as takeoff and turning operations. In addition, storing surplus energy using fuel cells increases the energy density and efficiency of the systems.

The operating voltage of fuel cells is variable and decreases as the load increases. On this basis, we constructed a hybrid system by using the voltage balance between a fuel cell and battery. A hybrid power management system was fabricated with a 11.1-V Li battery whose fully charged voltage (12.5 V) is identical to that of the normal output voltage of the fuel cell. Fig. 2 shows the electric circuit of a hybrid test module. The Li battery and fuel cell were connected to a DC-to-DC converter that regulated the output as 12 V. The DC-to-DC converter was directly linked by an electric load.

3. Results and discussion

3.1. Subsystem I: stack performance evaluation

The flow rate of hydrogen in the flow-through mode was calculated as 1.6 of the equivalence ratio. In the flow-through mode, 1.6 l min⁻¹ was fed to obtain 80 W output, whereas only 1.16 l min⁻¹ was required in the dead-end mode, as shown as Fig. 3a. In addition, in the dead-end mode with purge, another

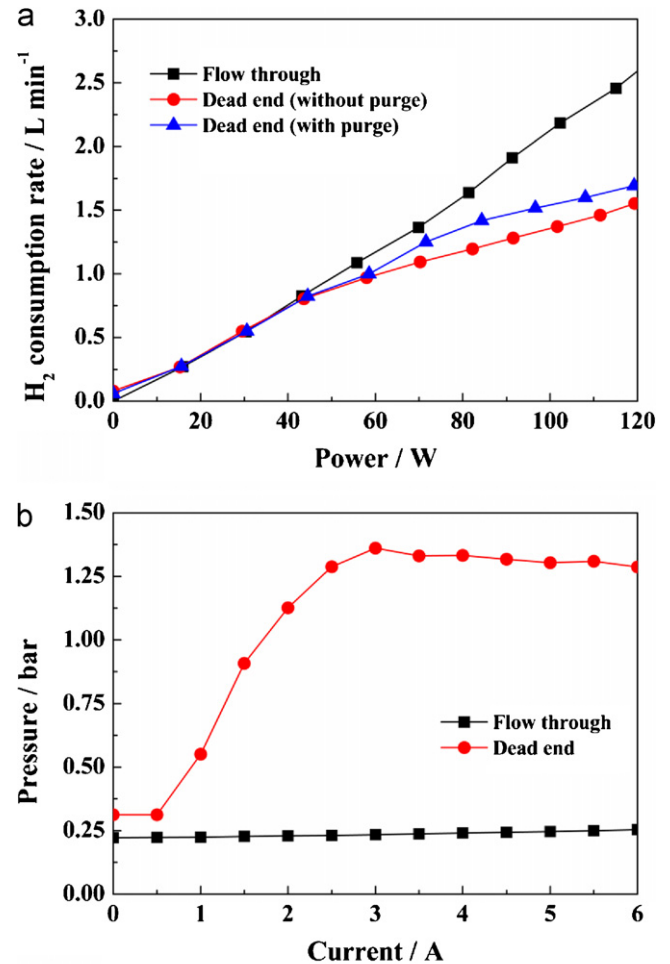


Fig. 3. Comparison of operating conditions with two operating modes (flow-through and dead-end): (a) hydrogen consumption rate and (b) operating pressure.

0.18 l min⁻¹ of hydrogen, corresponding to 0.338 g min⁻¹ of 15 wt.% NaBH₄ alkaline solution, was consumed to prevent flooding. The operating pressure was 0.22 bar and 1.3 bar in the flow-through and dead-end modes, respectively. Fig. 4 describes performance characteristics for the two operating modes during long test periods. The performance in the case of dead-end mode was significantly less than that in the case of the flow-through mode, because impurities such as water and nitrogen were accumulated in the cells. However, the performance in the case of the flow-through mode was not consistent due to flooding effects even though the excess hydrogen helped in impurities emission. Finally, even though the use of purge valves increased the total system weight and hydrogen

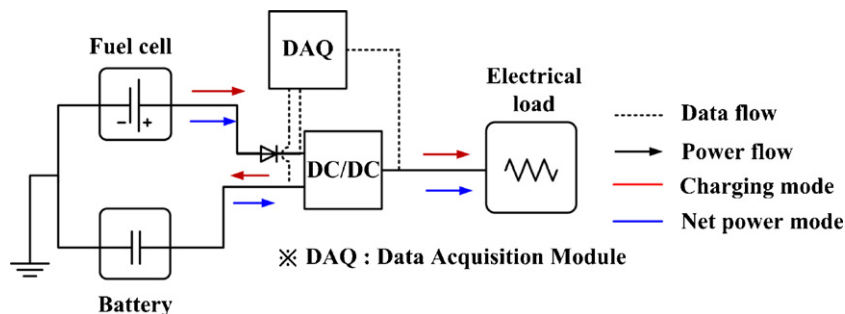


Fig. 2. Schematic diagram of power management test circuit.

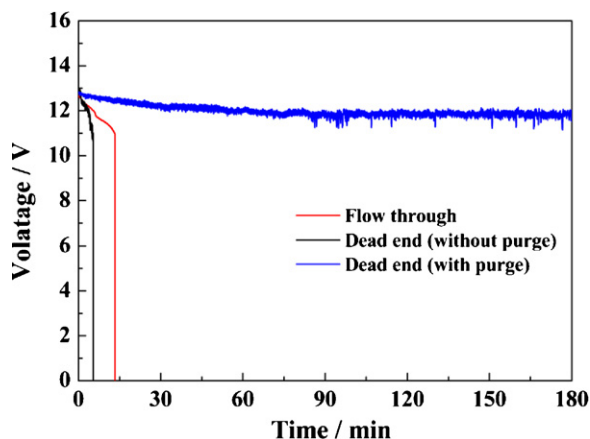


Fig. 4. Comparison of long-time output performances with the operating modes: 100 W, constant power mode; purge, 10 s.

consumption in the dead-end mode, purge was essential to ensure stable performances of the stack over long periods.

3.2. Subsystem II: hydrogen generator fabrication

3.2.1. Activation energy of $\text{Co}/\text{Al}_2\text{O}_3$

We fabricated a PTFE transparent reactor for catalytic hydrolysis. The weight fraction of the fabricated $\text{Co}/\text{Al}_2\text{O}_3$ was 28.24 wt.%. The catalytic hydrolysis reaction of NaBH_4 was dominantly affected by the reaction temperature. The hydrogen generation rate increased at high temperatures, while the kinetic reaction was a zero order reaction. We carried out the activation energy calculation of the NaBH_4 solution hydrolyzed by $\text{Co}/\text{Al}_2\text{O}_3$. The activation energy can be obtained by Arrhenius equation as follows:

$$k = k_0 \exp\left(\frac{-E}{RT}\right) \quad (3)$$

Here k is the reaction rate ($\text{ml min}^{-1} \text{g}^{-1}$); E_a , the activation energy for the reaction (kJ mol^{-1}); R , the gas constant ($8.314 \text{ kJ mol}^{-1} \text{ K}^{-1}$); and T , the reaction temperature (K). Fig. 5 presents the Arrhenius plot of the catalytic hydrolysis reaction of NaBH_4 alkaline solution by a $\text{Co}/\text{Al}_2\text{O}_3$ catalyst. The activation energy was calculated as $51.75 \text{ kJ mol}^{-1}$ by using the slope of the graph. This value can be compared with 47 kJ mol^{-1} and 61.1 kJ mol^{-1} for a Ru catalyst supported on IRA-400 and graphite, respectively [10,11]. Further, the activation energy of the $\text{Co}/\text{Al}_2\text{O}_3$ catalyst was distinguished in 48.1 kJ mol^{-1} of the Co-P catalyst [12].

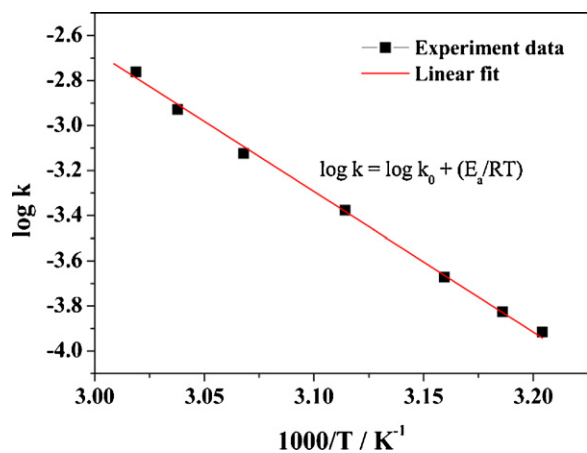


Fig. 5. Arrhenius plot for the activation energy calculation of $\text{Co}/\text{Al}_2\text{O}_3$ catalyst: 15 wt.% NaBH_4 , 5 wt.% NaOH .

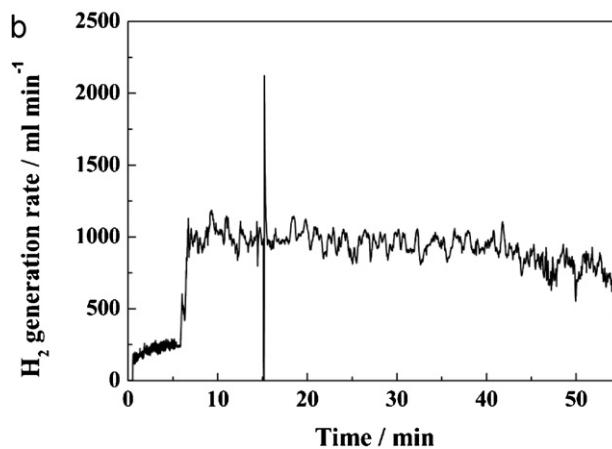
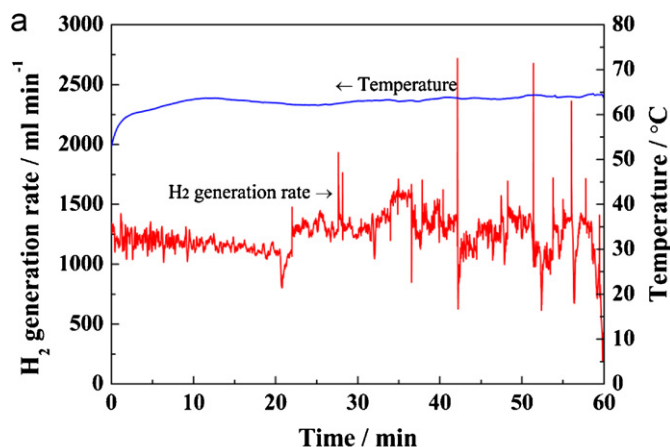


Fig. 6. Hydrogen generation performances by hydrogen generator: (a) flow rate fluctuations due to clogging by catalyst particles; (b) flow rate stabilized by a mesh filter; 15 wt.% NaBH_4 ; 5 wt.% NaOH ; flow rate, 3 ml min^{-1} .

3.2.2. Integration of hydrogen generator

The hydrogen generator performance was evaluated by measuring the flow rates of hydrogen. Fig. 6a shows the instability of the hydrogen generation rate as a result of clogging in the hydrogen flow channel. The pressure in the catalyst support pores sharply increased during the NaBH_4 hydrolysis reaction due to the phase conversion from liquid NaBH_4 to gaseous H_2 . The increased pressure crushed and washed the support, and the flow field was clogged with the support particles. In addition, the hydrogen generation rate exceeded the desirable value, 1 l min^{-1} , since the feeding rate of the NaBH_4 solution was affected by the sudden pressure fluctuations. The hydrogen generation rate became stabilized as shown in Fig. 6b after a mesh filter was installed to prevent the clogging phenomenon. The average hydrogen generation rate was 946 ml min^{-1} ; this is 11% lower than the theoretical value and this is probably because the actual feeding rate of the NaBH_4 solution by the pump was reduced to less than the setting value due to the effects of the reactor pressure. The feeding rate compensated for the shortfall in the reactor pressure of 1.2 bar, and accordingly, the hydrogen generation rate was stable and sufficient to operate the stack during the UAV's cruising mode (described in the next section).

3.3. Subsystem III: hybrid power management system

The performance tests were classified into 3 steps: (a) charging mode; (b) cruising mode; and (c) hybrid mode, as shown in Fig. 7. We limited the maximum output power of the fuel cell to 40 W. The consumption power at the electric load, P_l , was initially set as

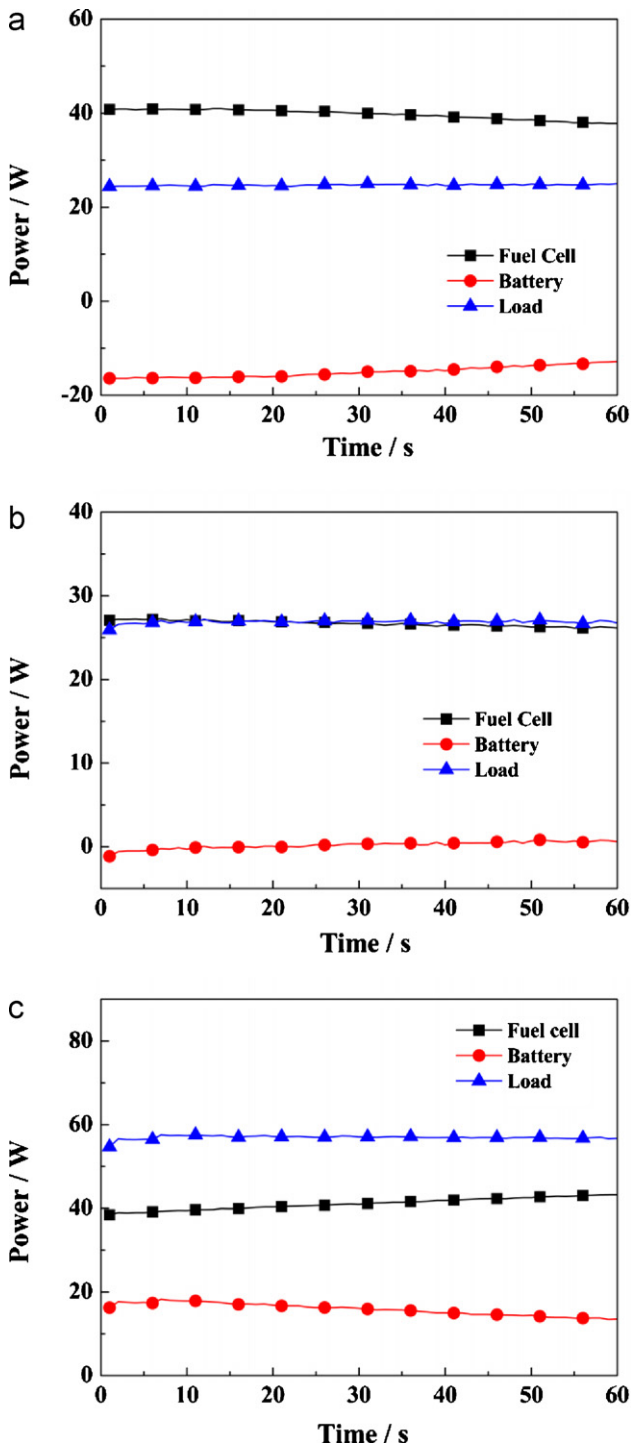


Fig. 7. The characteristics of hybrid power management system: (a) charging mode; (b) cruising mode; and (c) hybrid mode.

25 W, while the fuel cell output, P_{fa} , was 40 W. The battery output, P_b , was 15 W, and its power flow direction was negative. This meant that the surplus energy of the fuel cell was used to charge the battery, since the battery voltage was less than that of the fuel cell. As the battery was charged, the fuel cell output and charging rate decreased, since the difference between the voltages of the battery and fuel cell reduced. $P_b = 0$ implies that the battery voltage was identical to the fuel cell voltage and the battery was in a fully charged state, because the fully charged voltage of the battery was set as the output voltage of the fuel cell at maximum power.

At this point, if P_l is lower than 40 W, P_{fa} decreases below 40 W and equals P_l (see Fig. 7b); this is the cruising mode of the hybrid power management system. The UAV was powered only by the fuel cell, and the battery was in a neutral state during the cruising mode. To evaluate the hybrid mode, P_l was set as 55 W, which is higher than the fuel cell's maximum output. In this case, the battery was discharged with 15 W because the voltage of the fuel cell decreased to less than that of the battery due to excessive load. Consequently, the hybrid power management system satisfied the normal power consumption for cruising and the peak power requirement for takeoff. The operating modes were determined by the voltage difference between the fuel cell and battery. Hence, the voltage of the fully charged battery should match that of the fuel cell at the normal output power for efficient hybrid power management.

3.4. Fuel cell system integration

The fuel cell system module comprised the following subsystems: (a) 100-W PEMFC stack; (b) hydrogen generator; and (c) hybrid power management system. We calculated the weight proportion of the components as shown in Fig. 8; the fuel weight was not considered. The stack had the greatest portion of the total weight (43%) and was immoderately weighty. The hydrogen generator and hybrid power management system were optimized in terms of weight with 30% and 13%. Fig. 9 shows the specific energy density of the total system in accordance with the concentration and mass of the NaBH_4 solution. The system energy density was improved by reducing the stack weight or increasing the concentration and mass of NaBH_4 . In the present study, the specific energy density of the fuel cell system with 15 wt.% NaBH_4 solution was 165 Wh kg^{-1} , which is comparable to that of Li battery.

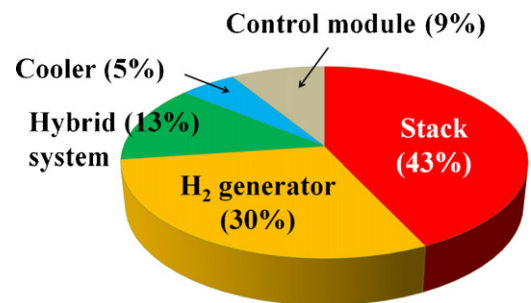


Fig. 8. Weight proportion of components in the fuel cell of unmanned aerial vehicle (UAV).

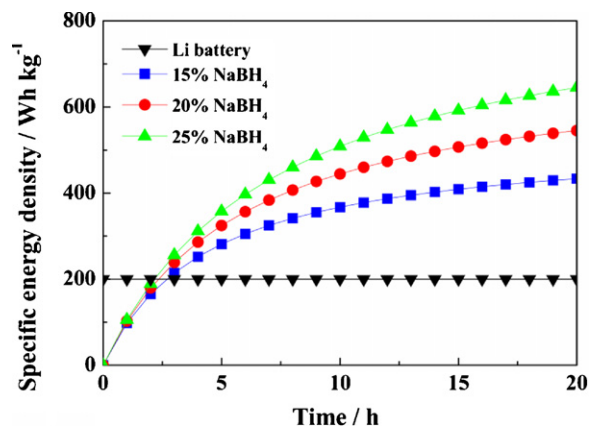


Fig. 9. Specific energy density estimation of fuel cell system: the fuel weight was not considered.

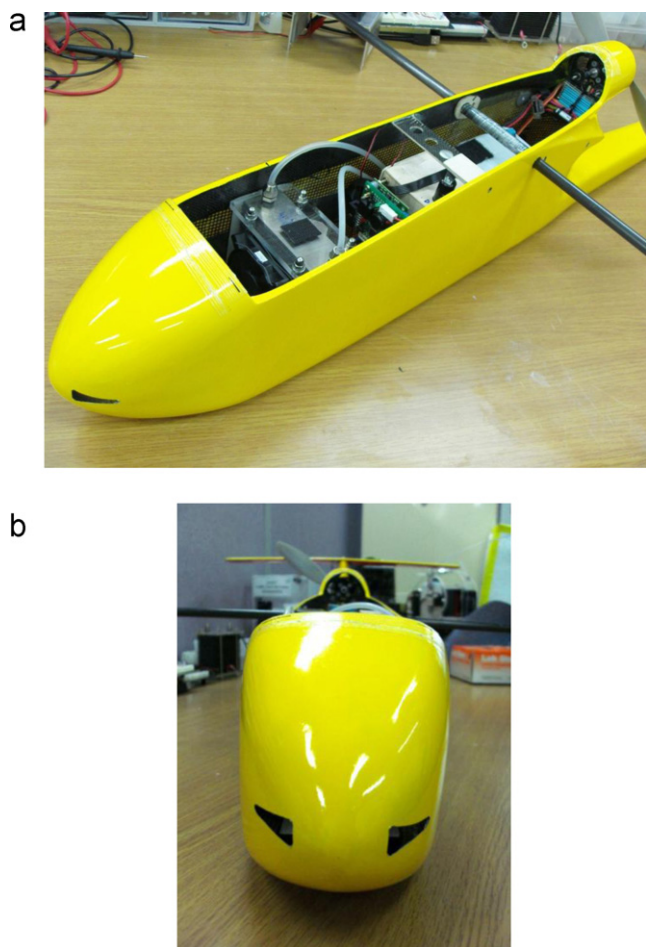


Fig. 10. Fabricated fuel cell UAV: (a) integration of fuel cell system into glider and (b) designed air intakes.

3.5. UAV integration and flight tests

The fuel cell system was integrated into the glider platform (see Fig. 10a). Furthermore, stack cooling is essential to ensure its performance. Water-cooling systems show good cooling capabilities but they are not appropriate for UAV applications since subsystems such as coolants, coolant tanks, and pumps are complex, bulky, and heavier. Hence, we recommend an air-cooling system for UAV applications since it consists of simple components and is light. Further, the cooling performance can be efficiently increased by using air induction in the cruising state. Air intakes (see Fig. 10b) and exits were designed using wind tunnel tests in order to use the air flow produced at the cruising state. Air flows through the intakes and cools the stack and other systems down. The heated air is emitted through the exits by the forced exhaust of the glider's propeller. An auto-pilot and an aerial camera, which were supported by NES & TEC Co. Ltd., were installed for auto-flights.

We performed ground tests and flight tests to evaluate the performance of the UAV and fuel cell system. In the ground tests, UAV maneuvering was controlled by a manual mode corresponding to power consumptions of 80 W. The operating time was 2.5 h with 360 g of 15 wt.% NaBH_4 solution. For the flight tests, UAV was launched by hand, and the auto-pilot controlled UAV's motions. Further, flight data such as flight speed, GPS coordinates, and altitude were monitored and recorded at the ground station. Fig. 11 shows the flight trajectory and altitude of the UAV. The trajectories have the form of a 50-m radius circle around which the ground station designated an arbitrary position for reconnaissance. The flight

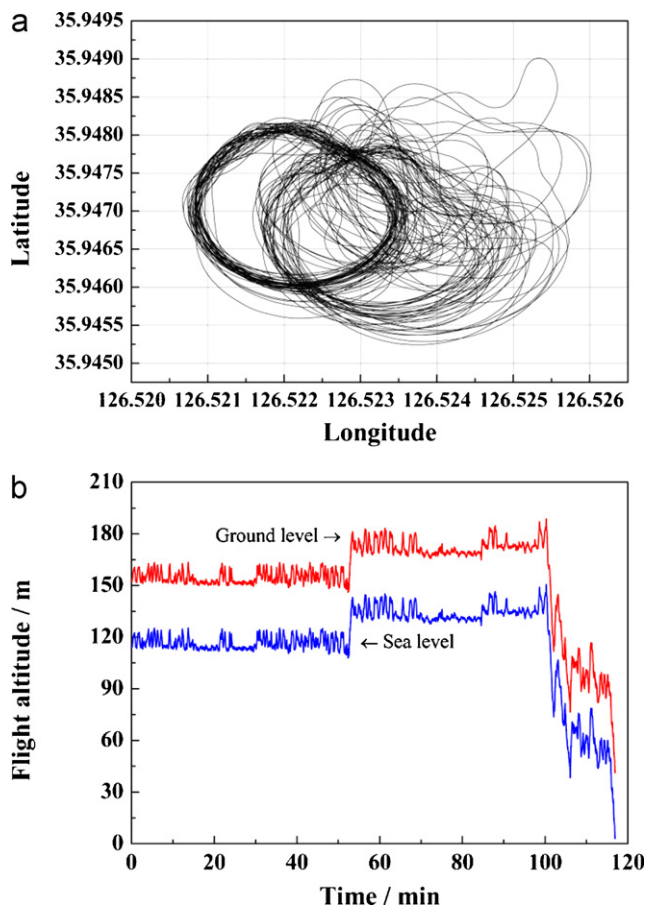


Fig. 11. Flight test results: (a) trajectory and (b) flight time vs. altitude.

altitude was set relatively low to scout the ground state by using the aerial camera. The flight endurance record was reduced in 2 h since circular flights require the continuous maneuvering. However, in this manner, we have been able to successfully achieve long-endurance flights of the UAV by using fuel cell systems in place of battery-powered UAVs.

4. Conclusion

We fabricated a fuel cell system using 15 wt.% NaBH_4 solution as the hydrogen source for a power source of UAV in order to improve the UAV's mission abilities. Hydrogen was generated by the catalytic hydrolysis of NaBH_4 . The primary subsystems comprising the components of the fuel cell system have been designed and evaluated. The fuel cell system was integrated into the UAV test platform, and flight tests were conducted to evaluate its performances. We have verified that fuel cell systems are more efficient power sources for long endurance flights of UAVs than batteries that have conventionally powered UAVs. It is essential to reduce the weight of stacks in order to increase the system energy density. Moreover, when the fuel capacity of UAV is upgraded, we can further improve the endurance of long flights for UAVs.

Acknowledgment

This work was supported by the Korea Science and Engineering Foundation (KOSEF) grant funded by the Korean government (MEST) through NRL (no. ROA-2007-000-20065-0).

References

- [1] E. Bone, C. Bolkcom, Unmanned Aerial Vehicles: Background and Issues for Congress, Congressional Research Service, Library of Congress, 2003.
- [2] B.A. Moffitt, T.H. Bradley, D.E. Parekh, D. Mavris, AIAA 44 (2006) 823.
- [3] F. Bairbir, PEM Fuel Cells: Theory and Practice, Elsevier Academic Press, New York, 2005.
- [4] J. Larminie, A. Dicks, Fuel Cell Systems Explained, 2nd ed., John Wiley & Sons, Chichester, 2003.
- [5] G. Cacciola, V. Antonucci, S. Freni, J. Power Sources 100 (2001) 67–79.
- [6] H.I. Schlesinger, H.C. Brown, A.E. Finholt, J.R. Gilbreath, H.R. Hockstra, E.K. Hyde, J. Am. Chem. Soc. 75 (1953) 215.
- [7] M.M. Kreevoy, R.W. Jacobson, Ventron Alembic 15 (1979) 2–3.
- [8] H.C. Brown, C.A. Brown, J. Am. Chem. Soc. 87 (1962) 1493–1494.
- [9] S.U. Jeong, R.K. Kim, E.A. Cho, H.J. Ha, S.W. Nam, I.H. Oh, S.H. Kim, J. Power Sources 144 (2005) 129–134.
- [10] S.C. Amendola, S.L. Sharp-Goldman, M.S. Janjua, M.T. Kelly, P.J. Petillo, M. Binder, J. Power Sources 85 (2000) 186–189.
- [11] Y. Liang, H.B. Dai, L.P. Ma, P. Wang, H.M. Cheng, J. Power Sources 35 (2010) 3023–3028.
- [12] X. Zhang, J. Zhao, F. Cheng, J. Liang, Z. Tao, J. Chen, J. Hydrogen Energy 35 (2010) 8363–8369.